High speed full range complex spectral domain optical coherence tomography

Erich Götzinger[1], Michael Pircher[1], Rainer A. Leitgeb[1,2], and Christoph K. Hitzenberger[1]

[1]*Center for Biomed. Eng. and Physics, Medical University of Vienna, Waehringer Str. 13, A-1090 Vienna, Austria*
[2]*Ecole Polytechnique Fédéral de Lausanne, Laboratoire d'Optique Biomédicale, CH-1015 Lausanne, Switzerland*
Christoph.Hitzenberger@meduniwien.ac.at

Abstract: We present a high speed full range spectral domain optical coherence tomography system. By inserting a phase modulator into the reference arm and recording of every other spectrum with a 90° phase shift (introduced by the phase modulator) we are able to distinguish between negative and positive optical path differences with respect to the reference mirror. A modified two-frame algorithm eliminates the problem of suppressing symmetric structure terms in the final image. To demonstrate the performance of our method we present images of the anterior chamber of the human eye in vivo recorded with an A-scan rate of 10000 depth profiles per second.

OCIS codes: (170.4500) Optical coherence tomography; (170.3880) Medical and biological imaging; (170.4470) Ophthalmology; (170.4580) optical diagnostics for medicine

References and links

1. D. Huang, E. A. Swanson, C. P. Lin, J. S. Schuman, W. G. Stinson, W. Chang, M. Hee, T. Flotte, K. Gregory, C. A. Puliafito, and J. G. Fujimoto, "Optical coherence tomography," Science **254** , 1178-1181 (1991).
2. A. F. Fercher and C. K. Hitzenberger, "Optical coherence tomography," Progress in Optics **44**, 215-302 (2002).
3. A. F. Fercher, W. Drexler, C. K. Hitzenberger, and T. Lasser, "Optical coherence tomography-principles and applications," Rep. Prog. Physics **66**, 239-303 (2003).
4. R. A. Leitgeb, C. K. Hitzenberger, and A. F. Fercher, "Performance of Fourier Domain vs. Time Domain optical coherence tomography," Opt. Express **11**, 889-894 (2003), http://www.opticsexpress.org/abstract.cfm?URI=OPEX-11-8-889.
5. J. F. de Boer, B. Cense, B. H. Park, M. C. Pierce, G. J. Tearney, and B. E. Bouma, "Improved signal to noise ratio in spectral domain compared with time domain optical coherence tomography," Opt. Lett. **28**, 2067-2069 (2003).
6. M. A. Choma, M. V. Sarunic, C. Yang, and J. A. Izatt, "Sensitivity advantage of swept source and Fourier domain optical coherence tomography," Opt. Express **11**, 2183-2189 (2003), http://www.opticsexpress.org/abstract.cfm?URI=OPEX-11-18-2183.
7. N. Nassif, B. Cense, B. H. Park, S. H. Yun, T. C. Chen, B. E. Bouma, G. J. Tearney, and J. F. de Boer, "In vivo human retinal imaging by ultrahigh speed spectral domain optical coherence tomography," Opt. Lett. **29**, 480-482 (2004).
8. A. F. Fercher, C. K. Hitzenberger, G. Kamp, and S. Y. El- Zaiat, "Measurement of intraocular distances by backscattering spectral interferometry," Opt. Commun. **117**, 43-48 (1995).
9. G. Häusler and M. W. Lindner, "Coherence radar and spectral radar - new tools for dermatological diagnosis," J. Biomed. Opt. **3**, 21-31 (1998).
10. M. Wojtkowski, R. Leitgeb, A. Kowalczyk, T. Bajraszewski, and A. F. Fercher, "In vivo human retinal imaging by Fourier domain optical coherence tomography," J. Biomed. Opt. **7**, 457-463 (2002).
11. A. F. Fercher, R. Leitgeb, C. K. Hitzenberger, H. Sattmann, and M. Wojtkowski, "Complex spectral interferometry OCT," Proc. SPIE. **3564**, 173-178 (1999).
12. M. Wojtkowski , A. Kowalczyk, R. Leitgeb, and A. F. Fercher, "Full range complex spectral optical coherence tomography technique in eye imaging," Opt. Lett. **27**, 1415-1417 (2002).
13. P. Targowski, M. Wojtkowski, A. Kowalczyk, T. Bajraszewski, M. Szkulmowski, and I. Gorczynska, "Complex spectral OCT in human eye imaging in vivo," Opt. Commun. **229**, 79-84 (2004).
14. R. A. Leitgeb, C. K. Hitzenberger, A. F. Fercher, and T. Bajraszewski, "Phase shifting algorithm to achieve high speed long depth range probing by frequency domain optical coherence tomography," Opt. Lett. **28**, 2201-2003 (2003).
15. R. N. Bracewell, *The Fourier transform and its applications, 3rd ed.* (McGraw-Hill, New York, 2000).

#5849 - $15.00 US Received 24 November 2004; revised 12 January 2005; accepted 15 January 2005

16. N. A. Nassif, B. Cense, B. H. Park, M. C. Pierce, S. H. Yun, B. E. Bouma, G. J. Tearney, T. C. Chen, and J. F. de Boer, "In vivo high-resolution video-rate spectral-domain optical coherence tomography of the human retina and optic nerve," Opt. Express **12**, 367-376 (2004), http://www.opticsexpress.org/abstract.cfm?URI=OPEX-12-3-367.
17. R. A. Leitgeb, W. Drexler, A. Unterhuber, B. Hermann, T. Bajraszewski, T. Le, A. Stingl, and A.F Fercher, "Ultrahigh resolution Fourier domain optical coherence tomography," Opt. Express **12**, 2156-2165 (2004), http://www.opticsexpress.org/abstract.cfm?URI=OPEX-12-10-2156.
18. B. Cense, N. A. Nassif, T. C. Chen, M. C. Pierce, S. H. Yun, B. H. Park, B. E. Bouma, G. J. Tearney, and J. F. de Boer, "Ultrahigh-resolution high speed retinal imaging using spectral-domain optical coherence tomography," Opt. Express **12**, 2435-2447 (2004), http://www.opticsexpress.org/abstract.cfm?URI=OPEX-12-11-2435.
19. M. Wojtkowski, V. J. Srinivasan, T. H. Ko, J. G. Fujimoto, A. Kowalczyk, and J. S. Duker, "Ultrahigh-resolution, high-speed, Fourier domain optical coherence tomography and methods for dispersion compensation," Opt. Express **12**, 2404-2422 (2004), http://www.opticsexpress.org/abstract.cfm?URI=OPEX-12-11-2404.
20. A. G. Podoleanu, G. M. Dobre, D. J. Webb, and D. A. Jackson, "Coherence imaging by use of a Newton rings sampling function," Opt. Lett. **21**, 1789-1791 (1996).
21. A. G. Podoleanu, G. M. Dobre, and D. A. Jackson, "En face coherence imaging using galvanometer scanner modulation," Opt. Lett. **23**, 147-149 (1998).
22. S. H. Yun, G. J. Tearney, J. F. de Boer, and B. E. Bouma, "Motion artifacts in optical coherence tomography with frequency domain ranging," Opt Express **12,** 2977- 2998 (2004), http://www.opticsexpress.org/abstract.cfm?URI=OPEX-12-13-2977.
23. American National Standards Institute: "American National Standard for Safe Use of Lasers," ANSI Z136.1-2000. Orlando, Laser Institute of America, 35-49 (2000).

1. Introduction

Optical coherence tomography (OCT) has developed to a powerful technique to image biological samples [1, 2, 3]. Recently it has been shown that spectral domain optical coherence tomography (SD-OCT) has significant advantages, in terms of acquisition speed and sensitivity, as compared to time domain optical coherence tomography (TD-OCT) [4, 5, 6]. A high speed SD-OCT system with an acquisition rate of 29300 depth profiles per second and a sensitivity of 98dB has been reported [7].

In spectral domain optical coherence tomography depth resolved information is encoded in the cross spectral density function measured with a spectrometer located in the detection arm of an interferometer [8, 9]. A drawback of this method is the presence of coherent noise terms and a strong DC term. Another disadvantage of SD-OCT is that since the detected spectral density is a real function and therefore its Fourier transform is Hermitian, the reconstructed image is symmetrical about zero path difference. As a consequence one cannot distinguish between negative and positive optical path differences with respect to the reference mirror. These effects are of minor importance for measuring thin objects (e. g. retina), because the reference arm can be shifted to a position where the mirror images and DC terms do not affect the image of the measured object. In [10] it is shown, that it is sufficient to subtract the reference arm spectrum (or averaged reference arm spectra) from the measured signal to achieve shot noise limited and autocorrelation free images from the retina. However, if one wants to measure objects with larger depth extension where the whole measurement range is needed (e. g. anterior segment of the eye) the DC and mirror terms heavily decrease the image quality and make it difficult to interpret the collected data. Furthermore, the sensitivity decrease of SD-OCT with distance from the zero position [9] would make a differentiation between positive and negative distances highly desirable because this would allow to place the object within the most sensible measurement range near the reference mirror position.

Fercher et al. [11] first pointed out that this problem can be solved by measuring the phase of the spectral interferometric signal, thus providing access to the complex scattered field. These authors introduced a method based on five measurements at each sampling location to get rid of the DC and mirror terms and to double the measurement range. Wojtkowski et al. [12] were the first to apply this technique to ocular imaging in vitro. However since a phase stability over five measurements is required, this method is not

#5849 - $15.00 US Received 24 November 2004; revised 12 January 2005; accepted 15 January 2005

suitable for in vivo measurements. Targowski et al. [13] presented images of the human eye in vivo based on the use of three A-scans per measurement location. However their acquisition speed was 3.6 seconds per image (one image consists of 326 A-lines), a measurement time which makes it difficult to measure patients. Recently Leitgeb et al. [14] introduced a method based on only two measurements which shares most of the advantages of the 5 frame technique. The instrument reported in that work used a piezo mounted reference mirror for phase shifting. This posed severe limits to the measurement speed, preventing in vivo imaging. Furthermore, the original method has the disadvantage that structure terms exactly symmetrical to the reference mirror position are attenuated or suppressed.

In this paper we present a high speed SD-OCT system based on the two frame technique and on a very fast electro optic phase modulator. Furthermore, we report a modified two-frame algorithm that avoids the suppression of symmetric structure terms. To demonstrate the performance of our system we present images of the anterior chamber in vivo with an A-scan rate of 10000 depth profiles per second, thus improving the imaging speed of full range complex SD-OCT by more than one order of magnitude.

2. Theory

The principle of SD-OCT is based on the fact that the spectral amplitude of the backscattered wave equals the Fourier transform of the spatial distribution of the object scattering potential [2, 3, 8]. An inverse Fourier transform of the spectral amplitude would therefore directly provide the object structure. However, amplitude data are not directly accessible: In SD-OCT systems, light back reflected from the reference arm and light backscattered from different sample depths is, after re-combining at an interferometer beam splitter, spectrally dispersed by a spectrometer to obtain the spectral intensity $I(\nu)$. An inverse Fourier transform of the intensity, however, yields not the object structure but its autocorrelation [8]:

$$FT^{-1}\{I(\nu)\} = \Gamma_{rr}(\tau) + \sum_n \Gamma_{nn}(\tau) + \sum_{n\neq m} \{\Gamma[\tau + (\tau_m - \tau_n)] + \Gamma[\tau - (\tau_m - \tau_n)]\} + \sum_n \{\Gamma[\tau + (\tau_r - \tau_n)] + \Gamma[\tau - (\tau_r - \tau_n)]\}, \quad (1)$$

where the indices m, n run over different object scattering sites in depth, $\tau_{n,m}$ and τ_r are traveling times of light beams in the sample arm to interfaces n and m, and in the reference arm, respectively. They are related to respective distances z in sample and reference arms by $\tau_{n,m,r} = z_{n,m,r}/c$, where c is the speed of light in the respective medium. $\Gamma(\tau)$ represents the first-order electric field correlation function. For simplicity, we have assumed equal reflectivity of the n interfaces in the sample, and a spectral intensity $I(\nu)$ consisting of pure cosine terms with zero phase offset.

The first two terms on the right hand side of equation (1) are DC terms, representing the intensity of light directly back reflected or –scattered at the reference mirror and sample interfaces. The sum of the third term represents autocorrelation terms which are caused by mutual interference of waves scattered within the object. This term can be regarded as a coherent noise that, together with the DC terms, corrupt the true object structure in a reconstructed image. The sum of the last term contains the actual object structure.

The reconstructed object structure is symmetric about the position of the reference mirror (zero position) which can be seen by the fact that the field correlation function Γ occurs twice in the sum, with positive and negative sign of $(\tau_r - \tau_n)$. The reason for this is that the spectral density is a real function, therefore, its Fourier transform will be Hermitian [15]. The consequence is that the reconstructed image is not only corrupted by the DC and autocorrelation terms, but it will also contain a mirror image of the object, with symmetry about the reference mirror position. If an overlap of image and mirror image is to be avoided, only half of the available image depth can be used. This poses the following limitations [9]: (i)

#5849 - $15.00 US Received 24 November 2004; revised 12 January 2005; accepted 15 January 2005

the imaging depth of SD-OCT is limited by the spectrometer resolution, (ii) a tradeoff between imaging depth and depth resolution exists, and (iii) there is a decay of sensitivity with image depth. Typical imaging depths of SD-OCT systems are 1 - 3 mm, too low for imaging deeper structures as, e.g., the anterior chamber of the human eye.

A solution to this problem is to measure the spectral phase and obtain the complex scattered field whose inverse Fourier transform equals the true object structure [11]. To measure the spectral phase, typically 3 to 5 consecutive measurements of spectral intensity are performed, taken with phase shifts in increments of 90° [11-13]. This phase shift can be accomplished by slight shifts of the reference mirror. The disadvantage of this method is that several measurements are necessary which poses considerable demands on the phase stability of the instrument within the time interval needed to perform the 3 to 5 measurements.

Recently, an alternative method has been presented that requires only two successive measurements with a 90° phase shift between the two measurements [14]. The thus recorded spectral intensities can be regarded as quadrature components from which a complex spectral intensity can be generated:

$$\tilde{I}(\nu) = I(\nu) + iI(\nu, \Delta\phi = 90°), \tag{2}$$

where $I(\nu, \Delta\phi = 90°)$ represents the spectral intensity recorded after a phase shift of $\Delta\phi = 90°$. An inverse Fourier transform of this signal now yields a first complex time domain signal $\tilde{S}_1(\tau)$:

$$\tilde{S}_1(\tau) = FT^{-1}\{\tilde{I}(\nu)\} = DC + iDC + AC + iAC + 2\sum_n \Gamma[\tau + (\tau_r - \tau_n)], \tag{3a}$$

where $DC = \Gamma_{rr}(\tau) + \sum_n \Gamma_{nn}(\tau)$ and $AC = \sum_{n \neq m} \{\Gamma[\tau + (\tau_m - \tau_n)] + \Gamma[\tau - (\tau_m - \tau_n)]\}$ are the DC and autocorrelation terms of eq. (1). Similarly, the inverse Fourier transform of the complex conjugate spectral intensity signal yields a second complex time domain signal $\tilde{S}_2(\tau)$:

$$\tilde{S}_2(\tau) = FT^{-1}\{\tilde{I}^*(\nu)\} = DC - iDC + AC - iAC + 2\sum_n \Gamma[\tau - (\tau_r - \tau_n)]. \tag{3b}$$

We can now calculate the modulus of these signals to obtain real-valued time domain signals:

$$S_1(\tau) = \left|\tilde{S}_1(\tau)\right| = \sqrt{2}\,DC + \sqrt{2}\,AC + 2\sum_n \Gamma[\tau + (\tau_r - \tau_n)], \tag{4a}$$

$$S_2(\tau) = \left|\tilde{S}_2(\tau)\right| = \sqrt{2}\,DC + \sqrt{2}\,AC + 2\sum_n \Gamma[\tau - (\tau_r - \tau_n)]. \tag{4b}$$

These signals still contain the DC and autocorrelation terms, however, structure terms and their mirror terms are now separated. Signal S_1 contains the direct structure term, signal S_2 the mirror term. If we calculate the difference:

$$\Delta S(\tau) = S_1(\tau) - S_2(\tau) = 2\sum_n \Gamma[\tau + (\tau_r - \tau_n)] - 2\sum_n \Gamma[\tau - (\tau_r - \tau_n)], \tag{5}$$

we can eliminate the DC and autocorrelation terms and obtain a signal with positive intensities corresponding to the real structure and negative intensities corresponding to the

#5849 - $15.00 US Received 24 November 2004; revised 12 January 2005; accepted 15 January 2005

mirror image. We finally multiply the signal with the Heaviside step function $\Phi[\Delta S(\tau)]$ to obtain only the positive values that correspond to the real structure:

$$\Delta S^{+}(\tau) = \Phi[\Delta S(\tau)]\Delta S(\tau). \tag{6}$$

While the method described so far has the advantage of effectively eliminating DC, autocorrelation, and mirror terms with only two measurements, it also has a drawback: it suppresses real structure terms that are exactly symmetric about the reference mirror position. This can be seen, if we assume two signals located at τ_1 and τ_2 with $\tau_r - \tau_1 = -(\tau_r - \tau_2)$. In this case $\Delta S(\tau)$ will be zero in case of equal reflectivities of the two symmetric backscatterers (in case of different reflectivities, a reduced signal corresponding to the difference in reflectivities will be observed).

To overcome this problem, we use additional information inherently present in the acquired data to determine the position of symmetric real structure terms (as opposed to mirror terms). For this purpose we calculate the inverse Fourier transforms of the two acquired real-valued spectral intensities and obtain their modulus. We will show that the difference between these signals indicates the position of symmetric real structure terms. (In the following discussion, we will omit the DC and autocorrelation terms since they are not affected by the 90° phase shift and it is therefore evident that, after subtraction of the two Fourier transformed signals, the corresponding signal peaks will be removed). The two modulus signals (without *DC* and *AC*) M_1 and M_2 are:

$$\left| FT^{-1}\{I(\nu)\} \right| \rightarrow M_1(\tau) = \left| \sum_n \Gamma[\tau + (\tau_r - \tau_n)] + \sum_n \Gamma[\tau - (\tau_r - \tau_n)] \right|, \tag{7a}$$

$$\left| FT^{-1}\left\{I^{*}(\nu, \Delta\phi = 90°)\right\} \right| \rightarrow M_2(\tau) = \left| \sum_n \Gamma[\tau + (\tau_r - \tau_n)] - \sum_n \Gamma[\tau - (\tau_r - \tau_n)] \right|, \tag{7b}$$

and the absolute value of their difference:

$$\Delta M(\tau) = \left| M_1(\tau) - M_2(\tau) \right| \tag{8}$$

contains information on the location of symmetric sample structure terms. Two cases have to be considered:

(i) In case of an asymmetric sample structure, e.g., only a single sample interface located at τ_1, signals M_1 and M_2 will each have peaks located at $\tau = -(\tau_r - \tau_1)$ and $\tau = +(\tau_r - \tau_1)$, i.e., they will be both mirror symmetric and are exactly equal. The difference $\Delta M_{asym}(\tau)$ will be zero, indicating that no symmetric structure term was found.

(ii) In case of a symmetric sample structure, e.g., two interfaces located at τ_1 and τ_2 with $\tau_r - \tau_1 = -(\tau_r - \tau_2)$, the two signals will be:

$$M_{1,sym}(\tau) = 2\left| \Gamma[\tau + (\tau_r - \tau_1)] + \Gamma[\tau - (\tau_r - \tau_1)] \right|, \tag{9a}$$

$$M_{2,sym}(\tau) = 0, \tag{9b}$$

and the magnitude of their difference $\Delta M_{sym}(\tau) = \left| M_{1,sym}(\tau) - M_{2,sym}(\tau) \right|$ contains signal peaks at positions (and only at those positions) where symmetric sample structure is located. Since $\Delta M_{asym}(\tau)$ will always be zero, $\Delta M(\tau) = \Delta M_{sym}(\tau)$, i.e., $\Delta M(\tau)$ contains signal peaks only at symmetric sample structure terms.

#5849 - $15.00 US Received 24 November 2004; revised 12 January 2005; accepted 15 January 2005

We might now obtain the true object structure by adding signals $\Delta S^{+}(\tau)$ (sample structure with suppressed symmetric structure terms) and $\Delta M(\tau)$ (symmetric structure terms). However, in real cases the peaks of $\Delta M(\tau)$ will be, in general, smaller than what would be expected from the corresponding sample reflectivities. The reason is that in our simplified derivation of equation (9) we assumed zero initial phase offset in the cosine terms of $I(\nu)$. In general, however, there will be such offset values. The consequence is that the peaks in $\Delta M_{sym}(\tau)$ (and in $\Delta M(\tau)$) are smaller than indicated by eq. (9). Therefore, $\Delta M(\tau)$ will just be used to locate the positions of symmetric structure peaks, and the corresponding peak magnitudes will be taken from signal $S_1(\tau)$ and replace the corresponding values in $\Delta S^{+}(\tau)$. The final equation describing the true object structure $F(\tau)$ is:

$$F(\tau) = \Phi[-\Delta M(\tau)]\Delta S^{+}(\tau) + \Phi[\Delta M(\tau)]S_1(\tau), \tag{10}$$

where Φ is the Heaviside step function which is used to gate the symmetric structure terms of $S_1(\tau)$. In practical applications, a certain threshold value has to be applied to the gating process to avoid erroneously gated data points caused by noise (in this work, a constant threshold was used throughout an entire image).

3. Experimental setup

Figure 1 shows the experimental setup. A SLD emits a beam with a center wavelength at 821 nm and a bandwidth of 25 nm, corresponding to a coherence length of 12 µm. After being polarized, the beam illuminates a Michelson interferometer where it is split by a non polarizing beam splitter (NPBS) into a reference arm and a sample arm. In the sample arm the beam is scanned across the object by a galvo scanner. A phase modulator (with a phase modulation frequency variable from DC to 100 MHz) was inserted into the reference arm of the interferometer. The phase modulator consists of an electro optic crystal. By applying an appropriate voltage to the crystal a corresponding change in the extraordinary refractive index will occur. If the optical input is both linearly polarized and aligned with the extraordinary axis of the modulator crystal, the output will undergo a pure phase shift with no change in the state of polarization. During image acquisition, the electro optic phase modulator is driven with a rectangular wave signal at half the linescan frequency of the camera, thus enabling a phase shift in every other line. To achieve phase stability of the phase modulator during each A-scan, either each linescan has to be triggered with the signal from the input voltage of the phase modulator, or the input signal to the phase modulator has to be triggered with each linescan. In our setup the phase modulator was triggered by the linescan. For dispersion compensation a similar electro optic crystal (without applying a voltage) was added to the sample arm.

To ensure that the reference arm power is near the saturation limit of the linescan camera (thus providing maximum sensitivity), a variable neutral density filter was added to the reference arm. After the beams are recombined at the NPBS they are coupled into a single mode polarization maintaining fiber (PMF) and guided to a spectrometer. With a half wave plate in front of the input fiber coupler the polarization state is aligned parallel to one of the birefringent axes of the PMF to excite only one polarization mode in the PMF, thus propagating a single plane parallel polarization state to the spectrometer. The light emitted from the fiber tip was collimated by a fiber coupler with a focal length of 50 mm. In front of the spectrometer we added another half wave plate to adjust the linear output of the PMF to the efficiency maximum of the diffraction grating.

The spectrometer consists of a reflection grating (1200 lines/mm), a camera lens with a focal length of 200 mm, and a 2048 element line scan CCD camera with a pixel size of 14 x 14 µm^2 (Atmel Aviiva M2 CL 2014). The maximum line rate of the camera is 29 kHz and via camera link and a high speed frame grabber card (PCI 1428 National Instruments) data could be transferred continuously to a personal computer. The resolution of the camera is 12 bit per

#5849 - $15.00 US Received 24 November 2004; revised 12 January 2005; accepted 15 January 2005

pixel. Since a spectrometer collects data as a function of wavelength, but the Fourier transform relationship is between time (distance) and frequency (wavenumber), the wavelength dependent data are re-sampled by linear interpolation to be equidistant in frequency space [10].

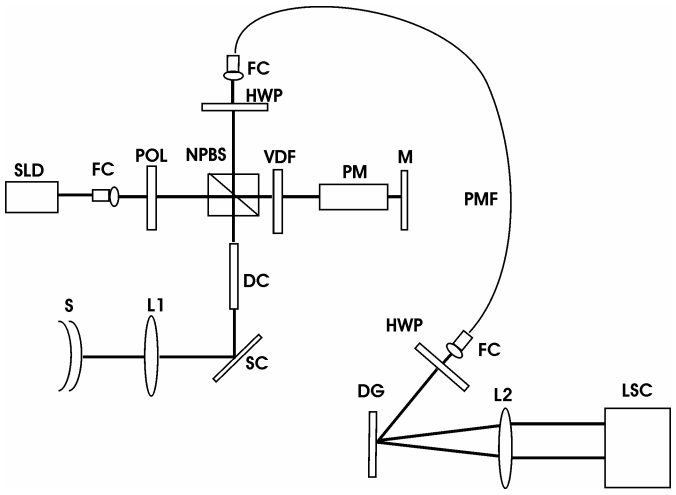

Fig. 1. High speed complex spectral domain optical coherence tomography system. SLD, superluminescent diode; FC, fiber coupler; Pol, polarizer; NPBS, nonpolarizing beamsplitter; VDF, variable density filter; PM, electro optic phase modulator; M, mirror; DC, dispersion compensation; SC, galvo scanner; L, lens; S, sample; HWP, half wave plate; PMF, polarization maintaining fiber; DG, diffraction grating; LSC, linescan camera.

We used an object lens L1 with a focal length of 80 mm and a beam diameter of 1.5 mm, providing a transversal resolution of 55 µm and a depth of focus of 5.7 mm. This large depth of focus was necessary to image the whole anterior chamber with approximately constant transverse resolution, independent of imaging depth, because in SD-OCT dynamic focusing is not possible.

SD-OCT has the advantage that no moving parts are necessary to obtain a depth scan. However, the achievable depth range Δz_{max} is given by the Nyquist limit of spectral resolution and is fixed by the spectrometer settings; i.e.: it depends on the wavelength resolution $\delta\lambda$ of the spectrometer and the center wavelength λ_0 of the light source [9, 10]. In normal SD-OCT systems $\Delta z_{max} = \lambda_0^2/(4\delta\lambda)$. In a full range complex SD-OCT system, this range is doubled. The measured depth range of our system is 2.95 mm with standard SD-OCT and 5.9 mm with complex SD-OCT, which is in good agreement with the design range of 6 mm. The sensitivity (ratio between the signal of a perfectly reflecting mirror and mean noise) of our system was 98 dB with an integration time of 100 µs and a power of 1.1 mW onto the cornea. This provided corneal images with a signal-to-noise ratio (SNR, defined as the ratio between the strongest signal obtained from the cornea and the mean noise) of 39 dB.

A considerable drawback of SD-OCT systems is the sensitivity decay along the axial measurement range [4, 9, 16]. This loss of sensitivity is caused by the finite spectral resolution of the spectrometer. Especially when the whole depth range is needed for imaging this strongly influences the image quality. In our system the sensitivity decay over ¾ of the measurement range was about 14 dB which is comparable to results published recently [16-19]. Therefore even at the periphery of the imaged depth field the sensitivity is 84 dB which is sufficient to image the whole anterior chamber. Our system worked with an A-scan rate of 10000 lines/sec, corresponding to 5000 complex lines/sec, and a nearly 100% duty cycle. A real time display of a reduced dataset of 1000 standard SD-OCT lines/sec could be used for alignment purposes, necessary for in vivo measurements. The computation time of calculating a full image consisting of 800 complex lines by our algorithm (cf. figure 3d) is presently 2 sec

#5849 - $15.00 US Received 24 November 2004; revised 12 January 2005; accepted 15 January 2005

(implemented in LabView, on a Pentium 4 processor operating at 3.2 GHz). An optimized routine written in C++ might work in real time.

4. Results

To test the performance of our system we made some measurements with a mirror as the sample. Figure 2 shows the results of the experiment. Figure 2a shows the reconstructed depth profile without applying the two frame algorithm (i.e., the inverse Fourier transform of real-valued spectrum $I(\nu)$). One can clearly see the strong DC term (which exceeds the range of the shown y axis), some fixed pattern noise, and the object peak and its mirror image located on both sides of the DC peak. Figure 2b shows signal S_1 (black curve), obtained from the complex spectrum, and signal S_2 (red curve), calculated from the complex conjugate spectrum.

Figure 2c shows signal $\Delta S = S_1 - S_2$. The DC term, the mirror image, and the fixed pattern noise terms are removed. The signal ΔS^+ displaying the object structure is obtained after multiplication of ΔS^+ by the Heaviside step function that eliminates the negative peak (fig. 2d). From fig. 2c one can easily imagine that symmetric structure terms (i.e., positive and negative peaks at the same abscissa position) would cancel each other.

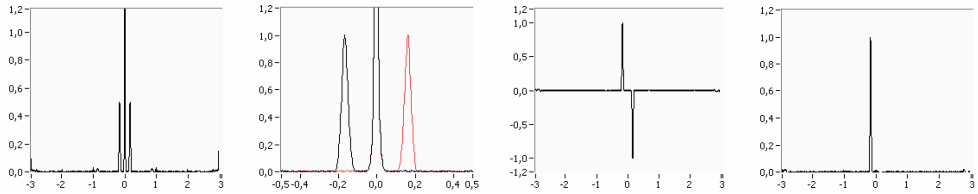

(a) (b) (c) (d)

Fig. 2. A-lines obtained from single reflecting surface (mirror attenuated by neutral density filter). Abscissa: distance (mm), ordinate: signal amplitude (linear scale, arbitrary units, normalized to amplitude of structure peak of signal S_1 in (b)). (a) Inverse Fourier transform of real-valued spectrum $I(\nu)$; (b) signals S_1 (black) obtained from complex spectrum and S_2 (red) obtained from complex conjugate spectrum (enlarged central section of depth profile); (c) difference signal $\Delta S = S_1 - S_2$; (d) final signal ΔS^+ (corresponds to final result of original two-frame algorithm).

To test the capability of our method to reconstruct the symmetric structure terms and thus be used to image scattering tissue with high speed in vivo, we imaged the human anterior chamber of a healthy volunteer. With a total of 1600 spectra per image (800 complex spectra equal to 800 full depth A-lines) the total recording time for one image was 160 ms. Figure 3 shows the results of these measurements.

After initial data processing steps comprising removement of the DC signal and fixed pattern noise (including a signal caused probably by internal reflection in the reference arm), and re-sampling the data to be equidistant in frequency space, fig. 3a was calculated by inverse Fourier transforming the real valued spectra $I(\nu)$. The overlapping mirror images are clearly visible. Furthermore residual DC and fixed pattern noise terms (straight vertical lines) can be seen. Hence it is difficult to recognize morphological details. In a next step the original two-frame technique [14] was applied, yielding signal $\Delta S^+(\tau)$, cf. fig. 3b. The mirror image is removed and the DC and fixed pattern noise terms are reduced. However, some shadow-like artifacts can be observed at positions where backscattering sites in the sample are symmetric with respect to the zero position (cf. areas where the real image of the cornea overlaps with its mirror image in fig. 3a; due to the statistical distribution of backscattering sites and intensities, there is no complete extinction of the corneal signals in these areas).

To eliminate these artifacts, the improved two-frame algorithm is applied. In a next step, we calculate signal ΔM (eq. (8)) to find the locations of the suppressed symmetric structure signals. ΔM is then used to gate signal S_1 to extract position and magnitude of the missing

#5849 - $15.00 US Received 24 November 2004; revised 12 January 2005; accepted 15 January 2005

structure signal. Figure 3c shows the suppressed structure terms found in this way. Finally, fig. 3d shows the true object structure $F(\tau)$ obtained by eq. (10). It equals the gated sum of figs. 3b and 3c. The shadows are essentially eliminated. (The residual vertical lines are probably caused by reflections within the reference arm because fixed pattern noise that is not affected by the phase shift between alternate A-lines is removed by the subtraction step of eq. (5)).

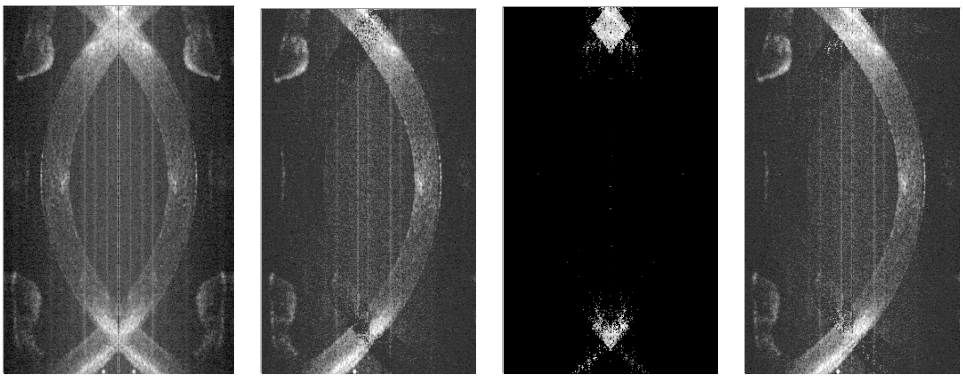

(a) (b) (c) (d)

Fig. 3. Images of anterior chamber of human eye in vivo. Size of imaged area: 5.9 mm (horizontal, optical distance) x 8 mm (vertical); each image consists of 800 A-lines. Logarithmic intensity scale. (a) Image obtained from inverse Fourier transform of real-valued spectrum $I(\nu)$, mirror terms corrupt the image. (b) Image corresponding to signal ΔS^{+} (original two frame algorithm); mirror terms are removed, shadow like artifacts remain. (c) Symmetric structure terms recovered by new algorithm. (d) Final image (gated sum of (b) and (c)) obtained by enhanced two-frame algorithm.

5. Discussion

In this paper we presented a high speed complex SD-OCT system, based on a very fast electro optic phase modulator. An imaging speed of 10000 A-lines/s equivalent to 5000 complex full range A-lines was achieved. This is an improvement of more than one order of magnitude as compared to previously reported complex SD-OCT. A further advantage of using an electro optic phase modulator is that this device is not limited to sinusoidal phase shifts at high frequency (as mechanically moving mirrors are due to their inertia). Since the cutoff frequency of the phase modulator is 100 MHz, it is able to support all the higher harmonics necessary to generate smooth, high frequency rectangular waveforms which fulfill the requirements of the phase shifting method better than a sinusoidal wave form.

The modified two-frame technique presented in this paper solves a problem of the original version of the algorithm, the suppression of symmetric structure terms. Although the original version provides images that can be used to derive the shape of the different structures of the anterior chamber and to determine the boundaries of, e.g., iris and cornea with great accuracy (cf. fig. 3b), the shadows observed at object structures symmetric to the zero position degrade the image quality and prevent a quantitative determination of signal intensities. These image artifacts are likely to be more critical in strongly scattering tissue. The new, enhanced algorithm solves this problem. The quantity $\Delta M(\tau)$ is used to determine the locations of symmetric structure terms. It should be pointed out that the measured value of $\Delta M(\tau)$ cannot be used directly as a measure of the signal magnitude of these symmetric terms. The reason is that the measured value of ΔM deviates from the value provided by eq. (8) by a factor that depends on the initial phase offset of the cosine terms of which $I(\nu)$ consists (the phase offset was assumed to be zero in the derivation of eq.(8)). This factor varies between 1 (zero phase offset) and 0 (45° phase offset). Therefore, $\Delta M(\tau)$ is just used to locate the positions of the symmetric structure terms; their values are obtained by gating signal $S_1(\tau)$

#5849 - $15.00 US Received 24 November 2004; revised 12 January 2005; accepted 15 January 2005

with the positions where $\Delta M(\tau)$ exceeds a threshold larger than noise. Only in rare cases, where the initial phase offset of a cosine term in the real-valued intensity signal $I(\nu)$ will be close to 45°, the method might fail (because then ΔM will be zero). However, given the random distribution of backscattering sites in scattering tissue, only a very small fraction of data points will be missed for this reason, and in a logarithmic intensity plot, as usual in OCT, this effect will probably be negligible.

Although the phase shift provided by the electro optic phase modulator has the required rectangular waveform, there are additional sources of phase instabilities that can degrade the results. Before we discuss the different sources of phase errors, we analyze their possible consequences.

Our derivations in section 2 were based on a phase shift $\Delta\phi = 90°$ between alternate A-lines. Only in this case, the separation of structure and mirror terms in signals $S_1(\tau)$ and $S_2(\tau)$ will be perfect. If $\Delta\phi$ deviates from 90°, signal $S_1(\tau)$ will contain residual mirror terms, and signal $S_2(\tau)$ will contain residual structure terms. However, these residual terms in S_1 and S_2 have no influence on the suppression of the mirror image in the actually displayed signal $\Delta S^+(\tau)$ (or $F(\tau)$) (as long as the residual mirror term is not stronger than the real structure term). This can best be seen in an example where a large deviation from the ideal value of $\Delta\phi = 90°$ is introduced. Figure 4 shows such an example, where $\Delta\phi \cong 40°$ (sample: attenuated mirror). From fig. 4a, which shows signals S_1 and S_2, it can be seen that the residual mirror term has ~ half of the amplitude of the real structure term. After calculating ΔS (fig. 4b), the real structure term is reduced in height (by a factor of ~ 2), and a corresponding negative mirror term is observed. In a final step, ΔS^+ is calculated (fig. 4c). The negative mirror term is eliminated by the step function, the reduced structure term remains. This example shows that phase errors have no influence on the effectiveness of the algorithm to eliminate mirror terms. Instead, the effect of phase errors is to reduce the signal magnitude of real structure terms (because the residual mirror terms are subtracted). The consequence is a reduction of SNR. Simulations have shown that a phase error of 30° causes a SNR drop by 3 dB. This indicates that our algorithm is rather immune to small phase errors. If, on the other hand, very large phase errors occur (> 90°), real image and mirror image are reversed (cf. figure 5).

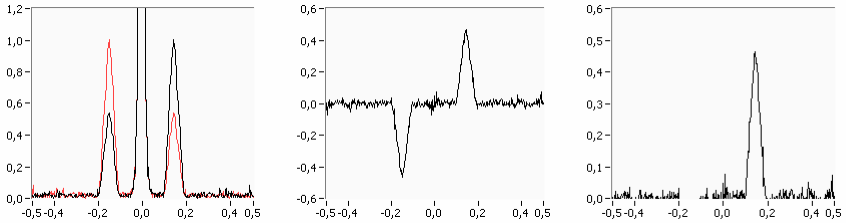

Fig. 4. Effect of phase error. A-lines obtained from single reflecting surface (cf. fig. 2). Abscissa: distance (mm), ordinate: signal amplitude (linear scale, arbitrary units, normalized to amplitude of structure peak of signal S_1 in (a)). (a) Signals S_1 (black) obtained from complex spectrum and S_2 (red) obtained from complex conjugate spectrum; (b) difference signal $\Delta S = S_1 - S_2$; (c) final signal ΔS^+ (corresponds to final result of original two-frame algorithm).

We now discuss possible sources of phase errors and the impact they might have on the results. One source of phase error can be interferometric jitter. However, since we use a very short integration time of 100 µs, this can easily be avoided. A second possible error source is polychromatic phase error. The phase shift introduced by the electro optic modulator depends on the wavelength. If a perfect 90° phase shift is introduced for the center wavelength λ_0, the shift will deviate from 90° for the other wavelengths of the broadband source. With $\lambda_0 = 821$ nm and $\Delta\lambda = 25$ nm, as used in our setup, the polychromatic phase error within the FWHM bandwidth will not exceed 1.4°. This can be neglected in the light of the previous discussion.

#5849 - $15.00 US Received 24 November 2004; revised 12 January 2005; accepted 15 January 2005

Another source of error is a phase change due to the galvanometer scanner movement between the two A-scans necessary to compute the complex signal. This effect has to be divided into two different sources of phase error. The first phase change arises from the sample path length variation with varying scanner angle. The sample path length shows a quadratic dependence on the angle of the scanner [20]. An additional phase change occurs, if the beam incident upon the scanning mirror does not fall on its axis of rotation [21]. This path length change depends on the off pivot point distance and on the angle of the scanner. The corresponding phase instabilities can be quite large. The example shown in fig. 4 was taken from an experiment where the incident beam position on the scanner was not exactly the pivot point of the scanner.

To avoid SNR degradation, the incident beam onto the scanners has to be carefully adjusted, ensuring pivot point illumination. It is clear that the effect of scanner movement strongly depends on the scanner velocity and the integration time. Therefore measurements might be difficult to realize, where a fast scanner velocity is necessary (e. g. 3D measurements). Further quantitative investigations are necessary to look into this problem in more detail. One solution would be to drive the scanner with a stepwise waveform. However, up to now no scanners with an appropriate response time (due to the very short integration time used in modern SD-OCT systems) are available.

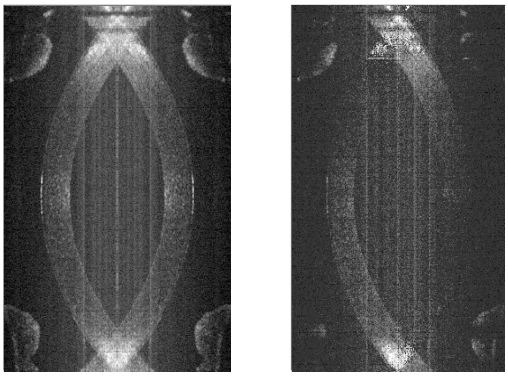

(a) (b)

Fig. 5. Image of human anterior chamber showing motion artifacts. Size of imaged area: 5.9 mm (horizontal, optical distance) x 8 mm (vertical); each image consists of 800 A-lines. Logarithmic intensity scale. (a) Image obtained from inverse Fourier transform of real-valued spectrum $I(\nu)$. (b) Image after applying two-frame algorithm.

A further source of phase errors are involuntary movements of the subject. In case of large movements, signals similar to those in figure 5 can be observed. The flip of the image approximately at its middle position occurred due to an involuntary movement of the subject which caused a phase error larger than 90°. In this case, signals S_1 and S_2 are switched, which, after calculation of ΔS^+, results in a flip of the image. This motion induced artifact must not be confused with the so called phase washout. A detailed description of this phenomenon can be found in [22].

The previous discussion has shown that some phase instabilities can be a problem with our technique. A possible solution to this problem will be to further decrease the integration time for one A-scan. Our camera allows integration times down to 35 µs. This should be possible without decreasing the signal to noise ratio, if the light power is increased. In our application, the light is focused on the cornea and divergent on the retina (divergence angle $\alpha \cong 19$ mrad). This corresponds to viewing of an extended light source, for which the ANSI standards [23] allow an illuminating power of ≅ 7.6 mW for illumination times > 15 s in the case of the parameters (λ, α) used in our setup.

#5849 - $15.00 US Received 24 November 2004; revised 12 January 2005; accepted 15 January 2005

In conclusion we presented a high speed experimental setup of a full range complex SD-OCT system using a 2 frame technique with the capability to measure 10000 A-scans per second. This is more than 20 times faster than previously published results [13, 14]. A modified two-frame algorithm prevents cancellation of symmetric structure signals. To demonstrate the possibility of in vivo measurements with this method, we presented images of the anterior chamber of a human eye in vivo with a recording time of 160 ms per image. The short imaging time allows to record images from the anterior segment without motion induced distortions. Nevertheless, decrease of sensitivity with depth is still a major problem of SD-OCT, especially when measuring thick tissue (e. g. anterior chamber). Future work will concentrate on possibilities to overcome this sensitivity decrease.

Acknowledgments

The authors wish to thank A. F. Fercher for helpful discussions on SD-OCT. H. Sattmann and L. Schachinger provided technical assistance which is gratefully acknowledged. Finally, financial assistance from the Austrian Fonds zur Förderung der wissenschaftlichen Forschung (FWF grant P16776-N02) is acknowledged.

#5849 - $15.00 US Received 24 November 2004; revised 12 January 2005; accepted 15 January 2005